Dalton Transactions

Accepted Manuscript

ROYAL SOCIETY OF CHEMISTRY

www.rsc.org/dalton

Final paper

Electrical transport and giant magnetoresistance in $La_{0.75}Sr_{0.25}Mn_{1-x}Cr_xO_3$ (0.15, 0.20 and 0.25) manganite oxide.

Ah.Dhahri[a,*], M.Jemmali[b], E.Dhahri[a], E.K.Hlil[c]

[a] Laboratoire de Physique Appliquée, Faculté des Sciences de Sfax, BP 1171, Université de Sfax, 3000, Tunisia.

[b] Laboratoire des Sciences des Matériaux et de l'Environnement, Faculté des Sciences de Sfax, BP 1171, Université de Sfax, 3000, Tunisia

[c] Institut Néel, CNRS et Université J. Fourier, BP 166, 38042 Grenoble, France

Abstract

We have investigated the influence of chromium (Cr) doping on the magneto-electrical properties of polycrystalline samples $La_{0.75}Sr_{0.25}Mn_{1-x}Cr_xO_3$ ($0.15 \leq x \leq 0.25$), prepared by sol-gel method. Comparison of experimental data with the theoretical models shows that in the metal-ferromagnetic region, the electrical behavior of the three samples is quite well described by a theory based on electron-electron, electron-phonon and electron-magnon scattering and Kondo-like spin dependent scattering. For the high temperature paramagnetic insulating regime, the adiabatic small polaron hopping (SPH) model is found to fit well the experimental curves.

Keywords: Conduction mechanism, small polaron hopping, magnetic materials, magnetoresistance, percolation theory.

*E-mail address: dhahri.ahmad@gmail.com

Tel: +216 20 20 45 55

1-Introduction

Colossal magnetic resistance (CMR) was discovered in the mixed-valence manganese oxides $Re_{1-x}M_xMnO_3$ (Re= rare earth, M =Sr, Ca, Ba) at a transition temperature close to that from a paramagnetic insulator (PMI) to ferromagnetic metal (FMM). This discovery has attracted much attention due to the extraordinary magnetic and electronic properties as well as the promise of the potential technological applications of these materials [1, 2]. So far, two CMR effects have been found in these manganites. They are the intrinsic CMR and extrinsic CMR. The intrinsic CMR is caused by the double exchange (DE) mechanism, which was proposed by Zener [3] in 1951. It is useful to explain the CMR phenomena observed near the Curie temperature (T_C) at a relatively high magnetic field (up to several kOe). The extrinsic CMR, which is related to the grain boundaries, can be explained by spin polarized tunneling [4]. The parent compound, $ReMnO_3$ is a charge-transfer (CT) insulator with trivalent manganese in different layers coupled among themselves antiferromagnetically through a superexchange mechanism. But within a layer, these Mn^{3+} ions are coupled ferromagnetically. When the Re trivalent element is doped by various elements, a proportionate amount of Mn^{3+} with the electronic configuration $\left(3d^4, t_{2g}^3 \uparrow e_g^1 \uparrow, S=2\right)$ is replaced by Mn^{4+} with the electronic configuration $\left(3d^3, t_{2g}^3 \uparrow e_g^0 \uparrow, S=3/2\right)$ creating holes in the e_g band[5]. The holes permit charge transfer in the e_g state, which is highly hybridized with the oxygen 2p state. According to Hund's rule, this charge transfer induces a ferromagnetic coupling between Mn^{3+} and Mn^{4+} ions which in turn has a dramatic effect on the electrical conductivity [6, 7]. It is believed that the study of the doping effects at the Mn site by other elements with different valences, electron configuration and ionic radius, is very important because of the crucial role of Mn ions in the CMR materials. The Mn-site doping is an effective way to modify the crucial Mn^{3+}-O^{2-}-Mn^{4+} network [8]. In turn, it remarkably affects the double exchange effect by modifying the interaction between Mn^{3+}/Mn^{4+}ions via O^{2-} ion network, which largely affects their physical properties as well as their CMR. So far, the magnetic ion substitution in the Mn-site and its effect on MR and MC properties has been extensively studied. Among the 3d-elements, Cr substitution is particularly interesting as Cr^{3+} is isoelectronic with Mn^{4+} and is a non-Jahn-Teller ion. In addition, the nature of the magnetic interaction between Cr^{3+}-O^{2-}-Mn^{3+} is known to favor ferromagnetism through superexchange interaction. It is of much

interest to know how the presence of a Cr ion in the Mn-site influences the magnetotransport and the MR properties of the material. Some models can explain the transport mechanism in manganites materials. However, most of them are only applied to fit the prominent change of the ρ-T curves in a finite temperature region (above or below T_C). On the one hand, the transport mechanism is explained by 3D Mott's variable range hopping (VRH) model, small polaron hopping (SPH) model and by the adiabatic small polaron hopping mechanism in the semiconductor region [9,10]. On the other hand, in the metallic region, the transport mechanism is governed by the single magnon's scattering contribution, the electron-magnon scattering mechanism, electron–electron and electron–phonon scattering processes [11-13].

In addition, a theoretical percolation model, proposed by Li et al., which is based on phase segregation between metallic and semiconductor regions, is used successfully in the whole temperature range [14].In view of these facts, a lot of efforts have been made to get insights into the effect of Cr^{3+} on the electrical properties of $La^{3+}_{0.75}Sr^{2+}_{0.25}Mn^{3+}_{0.75-x}Cr_xMn^{4+}_{0.25}O^{2-}_3$ ($0.15 \leq x \leq 0.25$). These materials show an important magnetoresistance effect near room temperature especially in the x=0.15 sample (MR= 59%, $T_{M\text{-}Sc}$=303K), which gives this compound the possibility of technologic application in the spintronic field at room temperature. The theoretical percolation model has been successfully used to explain the transport mechanism in the whole temperature range.

2-Experiment

The microstructure of ceramic materials in general and CMR materials in particular are highly affected by preparation routes and heat treatments. Sol-gel routes are known to produce very high quality, homogeneous and fine particle materials [15]. Bulk polycrystalline samples with compositional formula $La_{0.75}Sr_{0.25}Mn_{1-x}Cr_xO_3$ ($0.15 \leq x \leq 0.25$) were prepared by the sol-gel process. In this method, the metal nitrates taken in stoichiometric ratio were dissolved in an aqueous solution. Citric acid was added in 1:1 ratio and the pH was adjusted to a value between 6.5 and 7.0 by adding ammonia. After getting a sol on slow evaporation, a gelating reagent-ethylene glycol was added and heated between 160 and 180°C to get a gel. On further heating, this solution yielded a dry fluffy porous mass (precursor), which was calcined at 700°C for 6h. Then the powder was pressed into circular pellets. These pellets were sintered at 900°C in air for 12h. To obtain the metal-insulator transition temperature ($T_{M\text{-}Sc}$) and to study the influence of magnetic field on resistivity, the electrical resistivity and

magnetoresistance measurements have been done by standard dc four-probe technique using a closed cycle helium refrigerator cryostat in applied fields of 0T, 2T and 5T over a temperature range 4-400K.

3-Results and discussion

3.1. Magneto-transport behavior

A typical plot of resistivity (ρ) versus absolute temperature (T) in the case of $LSMCr_x$ (x=0.15, 0.2 and 0.25) at different fields is shown in figure 1. Change in resistivity around T_{M-SC} is interpreted in the framework of percolative conduction model based on the mixed phase of itinerant electrons and localized magnetic polarons. From figure 1, we can see that the resistivity at a given temperature is found to decrease with increasing field and that T_{M-SC} values are found to move towards the high temperature side with increasing magnetic field. The observed behavior may be attributed to the fact that the applied magnetic field induces the delocalization of charge carriers, which in turn suppresses the resistivity causing local ordering of the magnetic spins. Due to this ordering, the ferromagnetic metallic state may suppress the magnetic insulating regime. As a result, the conduction electrons (e_g^1) are completely polarized inside the magnetic domains and are easily transferred between the pairs $Mn^{3+}\left(3d^4, t_{2g}^3 \uparrow e_g^1 \uparrow, S=2\right)$ and $Mn^{4+}\left(3d^3, t_{2g}^3 \uparrow e_g^0 \uparrow, S=3/2\right)$ via oxygen. Hence the peak temperature (T_{M-Sc}) shifts to high temperature side with the application of magnetic field [16]. The percentages of magnetoresistance (MR) of all the samples have been calculated using the relation:

$$MR(\%) = \frac{\left(\rho(0,T) - \rho(H,T)\right)}{\rho(0,T)} \times 100 \qquad (1)$$

Where ρ(0, T) is resistivity under a zero magnetic field, ρ(H, T) is resistivity under an applied field. Figure 2 shows the variation of MR as a function of the temperature at different applied magnetic fields (2 and 5 T). The MR values of all the samples of the present work were calculated over a temperature range 4-450K, and maximum values of MR for each field were also calculated, and are given in table 1. It is interesting to note from table 1 that the samples with low T_{M-SC} exhibit large MR while those with high T_{M-SC} exhibit low MR, and the behavior is in agreement with the universal MR- T_{M-SC} relationship [17]. Our results are as important as earlier results. They even could be better in some cases (table1).

3.2. Electrical transport properties

First, we discuss electrical resistivity results with zero external magnetic field. Figure 1 shows the temperature dependence of electrical resistivity for $LSMCr_x$ samples. Taking the sign of the temperature derivative of the resistivity ($\frac{d\rho}{dT}$) as a criterion, we found that samples exhibit a metallic behavior ($\frac{d\rho}{dT} > 0$) at a low temperature ($T<T_{M\text{-}Sc}$) and become semiconductor-like

($\frac{d\rho}{dT} < 0$) above the temperature $T_{M\text{-}Sc}$, where $T_{M\text{-}Sc}$ is the temperature of the maximum value of resistivity ρ_{max}. For the samples x=0.15, 0.20 and 0.25, the transition temperatures $T_{M\text{-}Sc}$ occurs at $T_{M\text{-}Sc}$=303K, $T_{M\text{-}Sc}$=264K and $T_{M\text{-}Sc}$=231K respectively (table1), which are close to their Curie temperatures T_C (T_C= 317K, 278K and 253K) [18], indicating strong correlations between the magnetic and electrical properties in the $LSMCr_x$ samples. Therefore, we can define the ferromagnetic–metallic-like and the paramagnetic-semiconductor-like behaviors as a function of temperature.

The conduction in the FM phase ($T<T_{M\text{-}SC}$) is generally understood according to the DE theory. The Mn^{3+}-O^{2-}-Mn^{4+} coupling is responsible for the electrical conduction through charge transfer from the half-filled to the empty e_g orbital. The increase of the absolute value of resistivity with increasing the content of x, may be due to the decrease of the number of Mn^{3+}-O^{2-}-Mn^{4+} units and the increase of Cr^{3+}- O^{2-}-Cr^{3+}, Mn^{4+}- O^{2-}-$Cr^{3+}$and Cr^{4+}- O^{2-}-Cr^{4+}units which give rise to an antiferromagnetic temperature T_C, followed by the increase of the maximum of resistivity, ρ_{max}, in the $La_{0.75}Sr_{0.25}Mn_{1-x}Cr_xO_3$ samples. This constitutes further evidence of a weak DE interaction due to the increase of Mn^{4+}, Cr^{3+}, Cr^{4+}contents and the decrease of $<r_B>$.

3.2.1. Low-temperature behavior

In zero field measurements of resistivity, we can see from figure 3 that with decreasing temperature, the resistivity (ρ) increases up to metal-insulator transition temperature ($T_{M\text{-}Sc}$) and then decreases on further decrease of temperature and finally reaches a minimum value at about 35K (T_{min}). On further decrease of temperature below T_{min}, ρ is found to increase rapidly. This behavior is a characteristic feature of an insulator [19]. In contrast to the normally observed metallic behavior in the ferromagnetic region, the samples of the present

investigations are found to exhibit an insulating behavior. An obvious example can be seen in the insets of figure1 for 0T. In fact a similar type of behavior was reported earlier in other kinds of materials [20-22] and several theories were proposed to explain the observed anomalous behavior. Moreover, when the magnetic field is increased from 0 to 5T, the maximum of the resistivity decreases and $T_{M\text{-}Sc}$ shifts towards high temperature region. This may be due to the fact that the applied magnetic field delocalizes the charge carriers suppressing the resistivity, which cause local ordering of the electron spins. Due to this ordering, the ferromagnetic metallic state might have suppressed the paramagnetic insulating regime resulting in increasing $T_{M\text{-}Sc}$ values under the influence of magnetic field [23]. Further, T_{min} is found to shift towards low temperature region with increasing magnetic field which indicate the strong dependence of resistivity minimum on the magnetic field. The resistivity upturn below T_{min} is also found to suppress with increasing magnetic field. In view of these observations, the origin of this resistivity minimum at low temperature could be associated with the competition between weak localization effect, electron-electron scattering and electron-phonon scattering processes [24].

In spite of over a decade of intensive work on CMR materials, the variation of resistivity at low temperatures ($T<T_{M\text{-}Sc}$) and the relative strengths of different scattering mechanisms originating from different contributions are not yet thoroughly understood. Therefore, an attempt has been made to explain the low temperature regime, where the transport properties fully show the metallic state (below $T_{M\text{-}Sc}$) by fitting with the following equation, which is generally used to fit the electrical resistivity data in the case of manganites:

$$\rho(T) = \rho_0 + \rho_2 T^2 + \rho_{9/2} T^{9/2} \qquad (2)$$

Where ρ_0 arises from grain or domain boundaries. As the polycrystalline materials contain grains, grain boundaries and their significant contribution to the resistivity is proved in microwave measurements [25]. Hence, the term ρ_0 will play a major role in the conduction process. $\rho_2 T^2$in Eq. (2) indicates the resistivity due to the electron-electron scattering process and is generally dominant up to 100K [26,28]. Finally, the term $\rho_{9/2}T^{9/2}$ is a combination of electron-electron, electron-magnon and electron-phonon scattering processes [29, 30]. Actually, it is assumed that the latter process is more favorable in the half-metallic band structure materials such as manganites. However, as this model is not in a position to explain the low temperature upturn in the resistivity, it has been concluded that along with the above mentioned phenomena, some other factors might have also contributed to the low temperature

behavior. Based on the strong correlated effect in manganites, one has to consider the electron-electron interaction, which causes a $T^{1/2}$ dependence of resistivity in a disordered system [31]. Therefore, in order to explain the origin of the low temperature resistivity upturn, the experimental data have been analyzed by taking into account the electron-electron interaction, electron-phonon interaction, and Kondo-like scattering etc. Kondo effect was originally observed in diluted magnetic alloys and was attributed to the interaction between localized spins of magnetic impurities and the conduction electrons. To represent these phenomena, three more terms were included in Eq.(2) and the new equation is:

$$\rho(T)=\rho_0+\rho_e T^{1/2}-\rho_s \ln T+\rho_p T^5+\rho_2 T^2+\rho_{9/2} T^{9/2} \qquad (3)$$

Where the term $\rho_e T^{1/2}$ represents the contributions from correlated electron-electron interactions, while $\rho_s \ln T$ represents the contributions due to Kondo-like spin dependent scattering and finally $\rho_p T^5$ term is due to electron-phonon interactions.

The experimental resistivity data for $LSMCr_x$ samples were fitted to Eq. (3) and the quality of these fittings was evaluated by comparing the squared linear correlation coefficients (R^2). It is important to mention that the obtained values of R^2 for all samples were as high as 99.9%. Plots of the best fits to the data are shown by red solid lines in the main panels of figure 3 and the corresponding parameters are listed in table 2.

3.2.2. High-temperature behavior

The conductivity in the high temperature region ($T>T_{M\text{-}Sc}$), PI insulating phase is dominated by the hopping motion of self-trapped small polarons [32]. In order to explain the ρ-T in this region, we have used the adiabatic small polaron model given by the following expression: $\frac{\rho(T)}{T} = \rho_\alpha \exp\left(\frac{E_A}{k_B T}\right)$ (4)

Here E_A is the activation energy, k_B is Boltzmann's constant (~8.617×10^{-5}eVK^{-1}) and $\rho_\alpha = \frac{2k_B}{3ne^2a^2\vartheta}$ is the residual resistivity, 'e' is electronic charge, 'n' is the density of charge carriers, 'a' is site-to-site hopping distance, and 'ϑ' is the longitudinal optical phonon frequency. Figure 4 shows temperature dependent resistivity curves which have been obtained using small polaron model in the high temperature regime for the compounds studied in the present investigation. The activation energy values were obtained (table3) and are found to

increase with increasing Cr content. The increase in activation energy may be due to the fact that increase in Cr concentration lowers the possibility of conduction electron to hop to the neighboring sites [33]. On the application of magnetic field of 5T, activation energy values decrease for all the compounds of the present investigation. This may be attributed to decrease in the charge localization.

4. percolation model

Neither of the mentioned models can explain the prominent change of the ρ-T curves near $T_{M\text{-}Sc}$. Later Goodenough [32] showed that in CMR materials, a metallic conductivity exists in the ferromagnetic regions and a semiconductor-like conductivity above $T_{M\text{-}Sc}$ in the paramagnetic regions. Recently, based on the phase segregation mechanism [34], Li et al [35] proposed that the FM cluster and PM regions co-exist in CMR (percolation model) and that at any temperature, ρ is determined by the change of the volume fractions of the both regions. Under this scenario, the resistivity for the entire temperature range may be expressed as:

$$\rho = \rho_{FM} + (1 - f).\rho_{PM} \qquad (5)$$

Where f is the volume concentration of the FM region and $(1-f)$ is the volume concentration of the PM region. On the one hand, we can determine the function f by simple mathematical combination as: $f = \frac{\rho(T) - \rho_{PM}}{\rho_{FM} - \rho_{PM}}$. The volume fractions of FM and PM regions satisfy Boltzmann distribution:

$$f = \frac{1}{1 + \exp(\Delta U / K_B T)} \qquad (6)$$

And

$$1 - f = \frac{\exp(\Delta U / K_B T)}{1 + \exp(\Delta U / K_B T)} \qquad (7)$$

Where ΔU is the energy difference between FM and PM states, it may be expressed as $\Delta U \approx -U_0(1 - \frac{T}{T_C^{\mathrm{mod}}})$ (8). In this expression, U_0 is taken as the energy difference for a temperature well below T_C^{mod} (T_C^{mod} is a PM-FM transition temperature used in the model. It's near / equal to T_C).

From Eqs. (6), (7) and (8), one can find that,

- $f = 0 \, for \, T \ll T_C^{mod}, f = 1 \, for \, T \gg T_C^{mod} \, and \, f = f_C = \frac{1}{2} \, at \, T = T_C^{mod}$ [36]
- $1 - f = 1 \text{ for } T \ll T_C^{mod}, 1 - f = 0 \text{ for } T \gg T_C^{mod} \, and \, 1 - f = f_C = \frac{1}{2} \text{ at } T = T_C^{mod}$ [36]

Where f_C is the percolation threshold. To conclude, when f is less than f_C, the sample remains semiconducting and when f is larger than f_C it becomes metallic. Hence, the complete expression describing the temperature dependence of the electrical resistivity in the whole temperature range can be written in the form:

$$\rho(T) = \rho_0 + \rho_e T^{1/2} - \rho_s \ln T + \rho_p T^5 + \rho_2 T^2 + \rho_{9/2} T^{9/2} \times f + \rho_\alpha \, \mathrm{T} \exp\left(\frac{E_A}{k_B T}\right) \times (1 - f)$$

$$\rho(T) = (\rho_0 + \rho_e T^{1/2} - \rho_s \ln T + \rho_p T^5 + \rho_2 T^2 + \rho_{9/2} T^{9/2}) \times \frac{1}{1 + \exp\left(\frac{-U_0\left(1 - \frac{T}{T_C^{mod}}\right)}{k_B T}\right)}$$

$$+ \rho_\alpha \, \mathrm{T} \exp\left(\frac{E_A}{k_B T}\right) \times \frac{\exp\left(\frac{-U_0\left(1 - \frac{T}{T_C^{mod}}\right)}{k_B T}\right)}{1 + \exp\left(\frac{-U_0\left(1 - \frac{T}{T_C^{mod}}\right)}{k_B T}\right)} \qquad (9)$$

Eq. (9) may be used to examine our data over the whole temperature range both above and below T_C. The solid line in figure 5 shows the fitting results for the ρ-T curves obtained at zero-field, 2T and 5T for the samples x=0.15 and x=0.25. The best fit parameters are given in Table 4. It is worth mentioning that this percolation model is suitable to explain the electrical transport of $LSMCr_{1-x}$. Their excellent agreement confirms that FM domains and PM regions

coexist at near T_C. The temperature dependence on the volume concentration of the ferromagnetic phase f under different applied magnetic fields is shown in figure 6. When temperature is considerably below T_C, f is close to 1, but when temperature increases, at $T>T_C$, the concentration of the ferromagnetic phase approaches zero. The external magnetic field expands the concentration of the ferromagnetic phase, i.e., the concentration of the paramagnetic phase transfers into the ferromagnetic conductive regions under the influence of the external magnetic field, which leads to the increase in conductivity and the appearance of colossal magnetic resistance.

5. Conclusion

The electrical properties of $La_{0.75}Sr_{0.25}Mn_{1-x}Cr_xO_3$(x=0, 0.15, 0.2 and 0.25) have been studied. The electrical investigation show that metal-insulator transition temperature (T_{M-Sc}) decreases with an increase in Cr content. Large magnetoresistance of 74% at 5T field is achieved in the low-temperature region for x=0.25 sample. Analyses of the electrical transport data found that small polaron hopping (SPH) model is operative in the high temperature ($T > T_{M-Sc}$) regime in these manganites. Whereas the electrical conduction mechanism at low temperature ($T < T_{M-Sc}$) can be explained by a theory based on Kondo-like spin dependent scattering, electron-electron, electron-magnon, and electron-phonon scattering. Finally, to study the transport mechanism in the whole range of temperature, we have used the theoretical percolation model, including the ferromagnetic-metallic and paramagnetic-semiconductor states.

References

[1]L.Hueso,N.D.Mathur, Nature427(2004)303

[2]Md.M.Seikh, L.Sudheendra, C.N.R.Rao, J.Solid State Chem.177(2004)3633.

[3]C.Zener, Phys.Rev.82(1951)403.

[4]H.Y.Hwang, S.W.Cheong, N.P.Ong, B.Batlogg, Phys.Rev.Lett.77(1996)2041.

[5]K.Cherif, J.Dhahri, E.Dhahri, M.Oumezine, H.Vincent, J.Solid State Chem.163(2002)466-471.

[6]Z.Xinghua, L.Zhiqing, J.Rare earth2 9(2011)230-234

[7] L.Joshi, S.Keshri, Measurement 44(2011)938-945.

[8]J.L.Garcia,_Munoz, C.Frontera, P.Beran, N.Bellido, J.Hernandez-Velasco, C.Ritter, Phys.Rev.B81(2010)014409-014420.

[9] Dinesh Varshney, M.W. Shaikh. J. Alloy. Compd, 589 (2014) 558-567

[10]Dinesh Varshney, M.W. Shaikh, I.Mansuri J. Alloy. Compd, 486, (2009) 726-732.

[11]M.W. Shaikh, Dinesh Varshney. Mat Sci Semicon Proc 27(2014)418-426.

[12]A. Narjis, A. El kaaouachi, G. Biskupski, E. Daoudi, L. Limouny, S. Dlimi, M. Errai, A. Sybous. Mat. Sci. Semicon. Proc. 16 (2013) 1257–1261

[13] D. Varshney, D. Choudhary, M.W. Shaikh and E. Khan. Eur. Phys. J. B 76 (2010) 327–338.

[14] G. Li, H.D. Zhou, S.L. Feng, X.-J. Fan, X.G. Li, J. Appl. Phys. 92 (2002) 1406.

[15]P.N.Lisboa, A.W.Mombro, H.Pardo, E.R.Leite, W.A.Ortiz , Solid State Commun.130(2004)31.

[16]A.Banerjee, S.Pal, B.K.Chaudhuri, J.Chem.Phys.115(2001)1550-1559.

[17] A.P.Ramirez, J.phys: Condens. Matter 9 (1997) 8171.

[18] Ah.Dhahri, E.Dhahri,E.K.Hlil, Appl.Phys.A116(2014)2077-2085.

[19]S.Jin, T.H.Tiefel, M.McCromack, R.A.Fastnach, R.Ramesh, L.H.Chen, Science 264 (1994) 413.

[20]M.Auslender, A.E.Karkin, E.Rozenberg, G.Gorodetsky, J.Appl.Phys89(2001)6639.

[21]T.Sarkar, B.Ghosh, A.K.Raychaudhuri, T.Chatterji, Phys.Rev.B77(2008)235112.

[22]E.Rozenberg, M.Auslender, I.Felner, G.Gordetsky, J.Appl.Phys.88(2000)094407.

[23]G.Venkataiah, P.Venugopal Reddy, solid State Commun.136 (2005)114.

[24] L.Li, K.Nishimura, M.Fujii, K.Mori, solid State Commun.144 (2007)10.

[25]A.Urushibara,Y.Moritomo,T.Arima, A.samitsu, G.Kido,Y.Tokura, Phys.Rev.B51(1995)14103.

[26]P.T.Phong, N.V.Khiem, N.V.Dai, D.H.Manh, L.V.Hong, N.X.Phuc, J. Magn. Magn. Mater. 321(2009)3330-3334.

[27]M.Viret, L.Ranoo, J.M.D.Coey, Phys.Rev.B55(1997)8067-8070.

[28] Mohammed Wasim Shaikh, Dinesh Varshney Mater. Chem. Phys 134 (2012) 886-898.

[29]V.Sen, N.Panwar, G.L.Bhalla, S.K.Aguarwall, J.Phys.Chem.Solids.68(2007)1685.

[30]G.J.Snyder, R.Hiskers, S.Dicarolis, M.R.Beasley, T.H.Geballe, Phys. Rev. B53 (1996)14434-14444.

[31] M.Ziese, Phys.Rev.B68(2003)132411.

[32]J.B.Goodenough, J.S.Zhou, Nature 386(1997)229.

[33] A.Banerjee, S.Pal, S.Bhattacharya, B.K.Chaudhuri, J.Appl.Phys.91(2002)5125

[34] E. Dagotto, T. Hotta, A. Moreo, Phys. Rep. 344 (2001) 1.

[35] G. Li, H.D. Zhou, S.L. Feng, X.-J. Fan, X.G. Li, J. Appl. Phys. 92 (2002) 1406.

[36] M. Pattabiramana, G. Rangarajana, P. Murugaraj, Solid State Commun, 132 (2004) 7.

[37]Young Sun, Wei Tong, Xiaojun Xu, and Yuheng Zhang. Appl. Phys. 78(2001) 5.

[38]F. Elleuch , M. Triki , M. Bekri , E. Dhahri, E.K. Hlil. J. Alloy. Compd 620 (2015) 249–255.

[39] M. Khlifi, E. Dhahri, E.K. Hlil. J. Alloy. Compd 587 (2014) 771–777.

[40] N. Kallel ,K. Frohlich, S. Pignard, M. Oumezzine, H. Vincent . J. Alloy. Compd 399 (2005) 20–26.

[41] W. Cheikh-Rouhou Koubaa, M.Koubaa,A. Cheikhrouhou. J. Alloy. Compd. 453 (2008) 42–48

Tables caption

Table.1.Comparison of the values of magnetoresistance of $La_{0.75}Sr_{0.25}Mn_{1x}Cr_xO_3(0.15\leq x\leq 0.25)$ compounds (this work) with earlier results.

Table.2.The best fit parameters obtained from the experimental resistivity data of the metallic behavior (below $T_{M\text{-}Sc}$).

Table.3.Fitting parameters of the small polaron model for $La_{0.75}Sr_{0.25}Mn_{1x}Cr_xO_3(0.15\leq x\leq 0.25)$.

Table.4. Obtained parameters corresponding to the best fit to the Eq. 9 of the experimental data of $La_{0.75}Sr_{0.25}Mn_{1x}Cr_xO_3$ $(0.15\leq x\leq 0.25)$ at 0, 2, and 5 T.

Table 1

Samples	T_{M-Sc} (K)	MR(%) around T_{M-Sc} for 5T field	References
$La_{0.75}Sr_{0.25}Mn_{0.85}Cr_{0.15}O_3$	303	59	This work
$La_{0.75}Sr_{0.25}Mn_{0.8}Cr_{0.2}O_3$	264	65	This work
$La_{0.75}Sr_{0.25}Mn_{0.75}Cr_{0.25}O_3$	231	74	This work
$La_{0.67}Sr_{0.33}Mn_{0.9}Cr_{0.1}O_3$	340	30	[37]
$Pr_{0.5}\square_{0.1}Sr_{0.4}MnO_3$	211	25	[38]
$La_{0.8}Ca_{0.2}MnO_3$	250	48	[39]
$La_{0.7}Sr_{0.3}Mn_{0.9}Sn_{0.1}O_3$	225	11	[40]
$La_{0.7}Sr_{0.1}Ag_{0.2}MnO_3$	245	30	[41]

Table 2

Sample code	$\mu_o H$(T)	ρ_0(Ω.cm)	ρ_2($\times 10^{-6}$Ω.cm/K^2)	$\rho_{9/2}$($\times 10^{-11}$Ω.cm/K^2)	ρ_e(Ω.cm/K$^{1/2}$)	ρ_s(Ω.cm)	ρ_p($\times 10^{-6}$Ω.cm/K^5)
$LSMCr_{0.15}$	0	0.28861	20	5.7492	0.20219	0.1833	7.6442
	2	0.26752	19.5316	3.3578	0.04115	1.3233	2.6696
	5	0.25631	19.3256	1.626	0.03439	0.26295	1.7457
$LSMCr_{0.20}$	0	0,63169	12,8976	8.4965	0.4452	0.22168	4.57
	2	0,62457	11.6573	8.4792	0.2364	0.67357	4.374
	5	0.62183	10.5746	5.9099	0.20897	0.283	1.9499
$LSMCr_{0.25}$	0	0.91437	7.6973	12.176	0.6821	0.10187	7.4878
	2	0.83888	7.0698	6.9099	0.5482	0.19168	5.2957
	5	0.71051	5.8952	4.4068	0.50879	0.04594	2.6123

Table 3

Sample code	μ_0H(T)	ρ_α($\times10^{-6}\Omega$.cm)	E_a(meV)	R^2
$LSMCr_{0.15}$	0	22.9	61.29	99.95
	2	23.1	54.57	99.92
	5	29	22.93	99.97
$LSMCr_{0.2}$	0	11.9	102.25	99.95
	2	12.1	93.88	99.96
	5	22.4	82.09	99.96
$LSMCr_{0.25}$	0	7.82	242.42	99.98
	2	7.42	225.14	99.93
	5	9.44	200.16	99.94

Table 4:

Sample code	$LSMCr_{0.15}$			$LSMCr_{0.20}$			$LSMCr_{0.25}$		
	0 T	2 T	5 T	0 T	2 T	5 T	0 T	2 T	5 T
ρ_0 (Ω.cm)	0.28855	0.26755	0.25630	0.63171	0.62458	0.62186	0.91439	0.83891	0.7104
ρ_2 ($\times10^{-6}$ Ω.cm/K^2)	21	19.5322	19.3258	12.8973	11.6572	10.5751	7.6971	7.0696	5.8949
ρ_α (10^{-6}Ω.cm)	22.86	23.22	29.01	11.95	12.16	22.38	7.79	7.45	9.51
$\rho_{9/2}$($\times10^{-11}$ Ω.cm/K^2)	5.7491	3.3576	1.6261	8.4966	8.4789	5.9011	12.174	6.9012	4.4072
ρ_e (Ω.cm/$K^{1/2}$)	0.20201	0.04117	0.03441	0.4456	0.2361	0.20898	0.6823	0.5484	0.5088
ρ_s (Ω.cm)	0.1831	1.3236	0.26299	0.22167	0.67360	0.2833	0.10191	0.19172	0.0459
ρ_p ($\times10^{-13}$ Ω.cm/K^5)	7.6446	2.6693	1.7461	4.5731	4.3762	1.9511	7.4882	5.2963	2.6133
E_A/k_B (K)	711.26	633,28	266,10	1186,60	1089,47	952,65	2813,27	2612,74	2322,8
U_O/k_B (K)	3065	3088	3122	2040	2194	2288	1412	1759	1772
T_C^{mod}(K)	320	324	329	277	283	287	236	241	245
R^2 (%)	99.96	99.98	99.94	99.93	99.97	99.98	99.93	99.98	99.97

Figure captions

Figure.1. Temperature dependence of resistivity ρ(T) under different magnetic field for $LSMCr_x$ (x=0.15 and x=0.25).

Figure.2. Magnetoresistance plotted vs. temperature for $LSMCr_x$ (x=0.15, x=0,20 and x=0.25) samples under different magnetic field applied.

Figure.3 Theoretical fit of low temperature resistivity data for $LSMCr_x$ (x=0.15 and x=0.25). Symbols are the experimental results and the bold solid line in these plots represents the best fit of experimental data in the metallic regime, below $T_{M\text{-}Sc}$ with Eq.(2)

$$\rho(T)=\rho_0+\rho_e T^{1/2}-\rho_s \ln T+\rho_p T^5+\rho_2 T^2+\rho_{9/2} T^{9/2}$$

Figure.4. Theoretical fit of high temperature resistivity data for $LSMCr_x$ (x=0.15 and x=0.25).

Figure.5. The temperature dependence of resistivity for $LSMCr_x$ (x=0.15 and x=0.25) under various magnetic fields 0, 2 and 5T. Symbols are the experimental data and solid lines are the resistivity calculate using Eq. 9 corresponding to the parameters indicated in table 3.

Figure.6. the temperature dependence of ferromagnetic phase volume fraction f (T) for $LSMCr_x$ (x=0.15 and x=0.25) under applied magnetic fields 0, 2 and 5T.

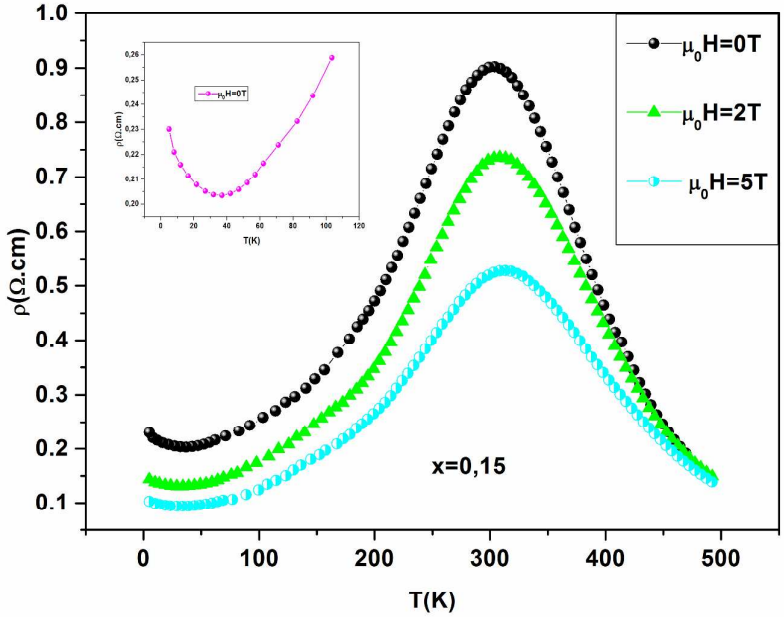

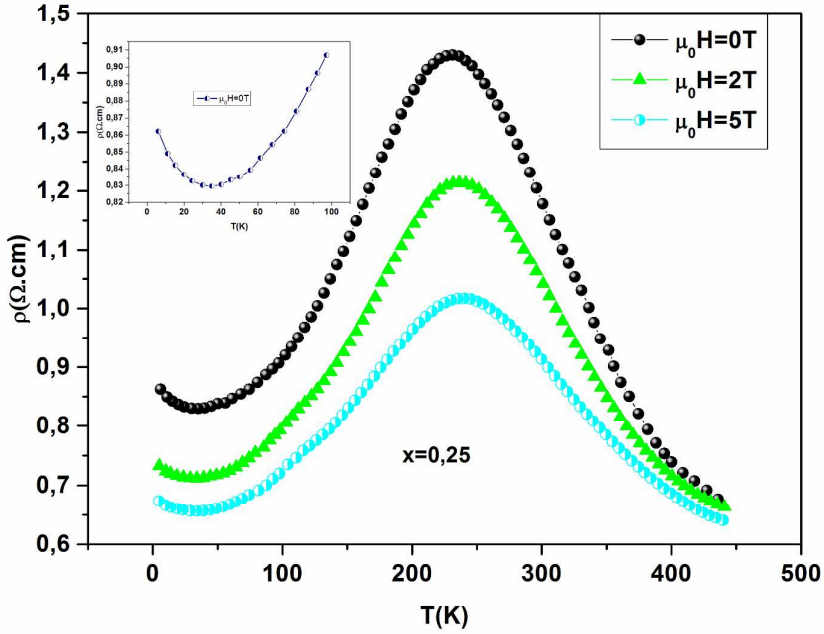

Figure 1

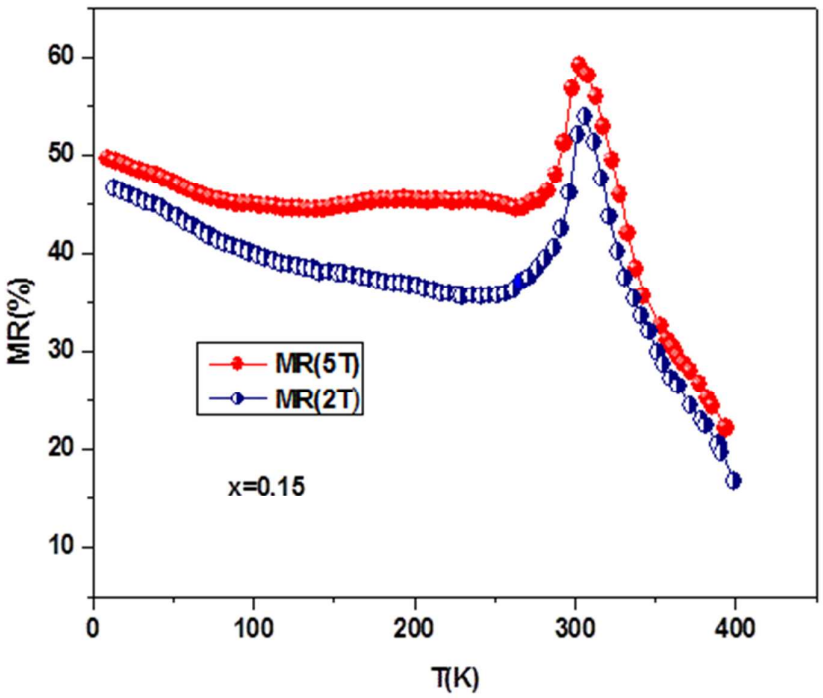

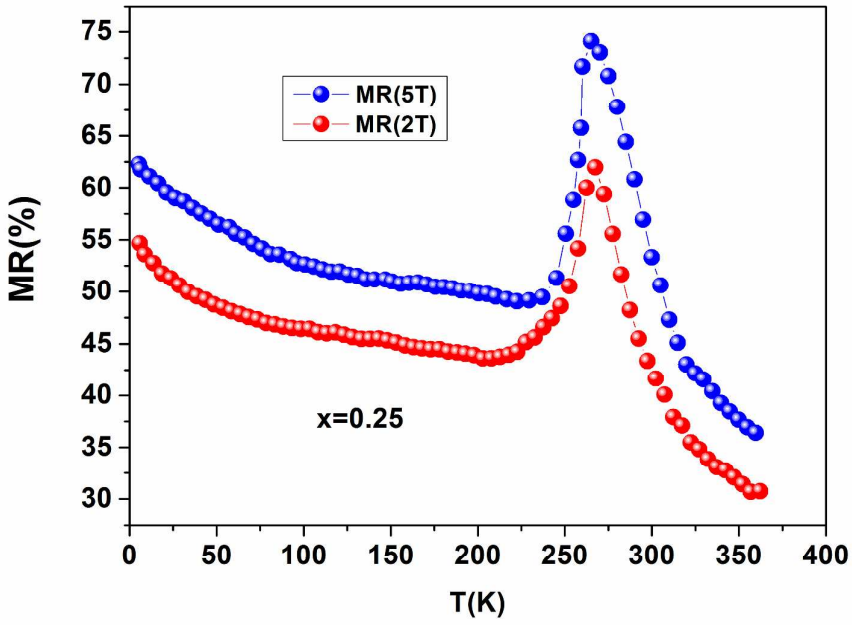

Figure 2

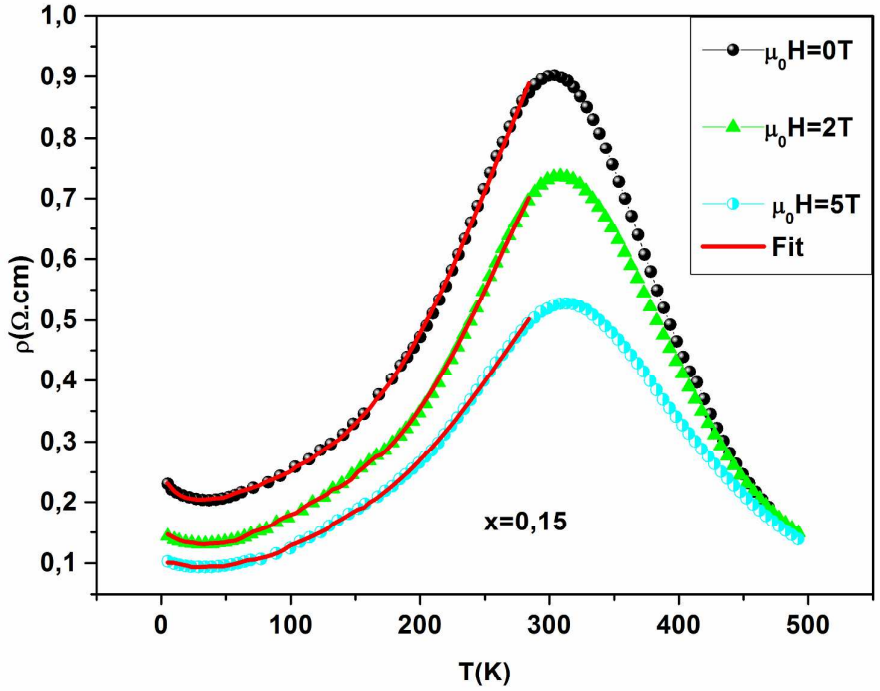

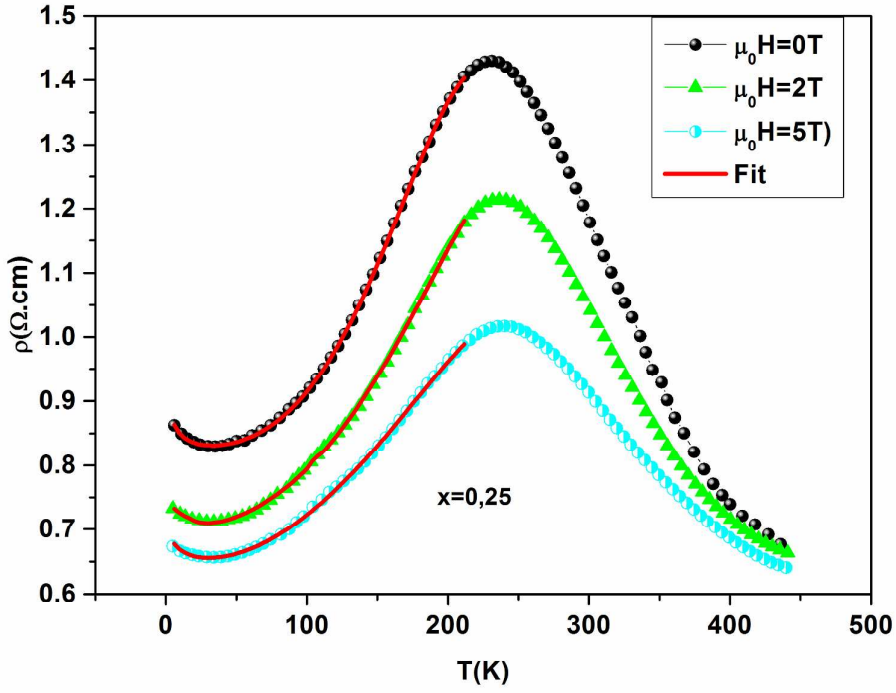

Figure 3

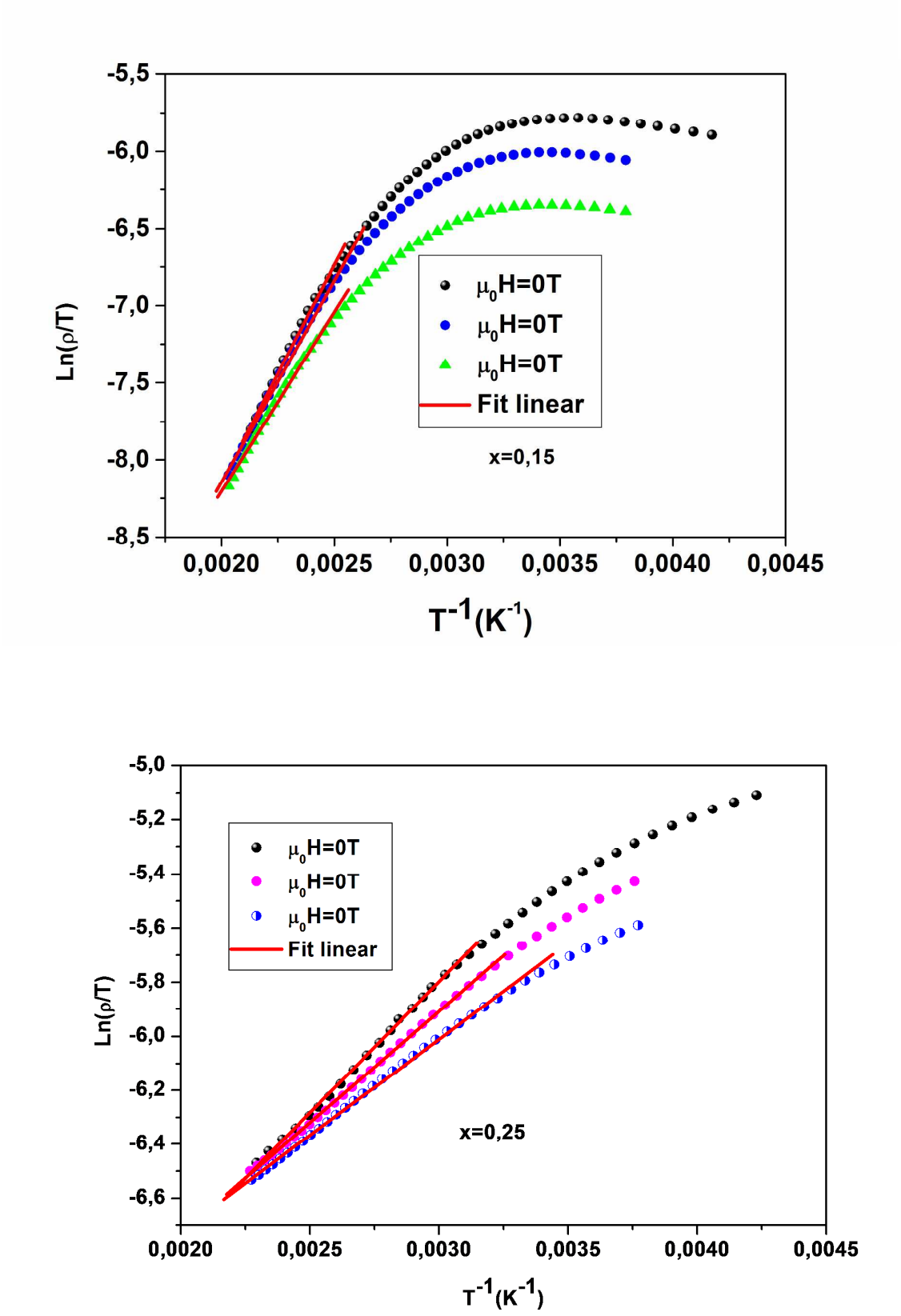

Figure 4

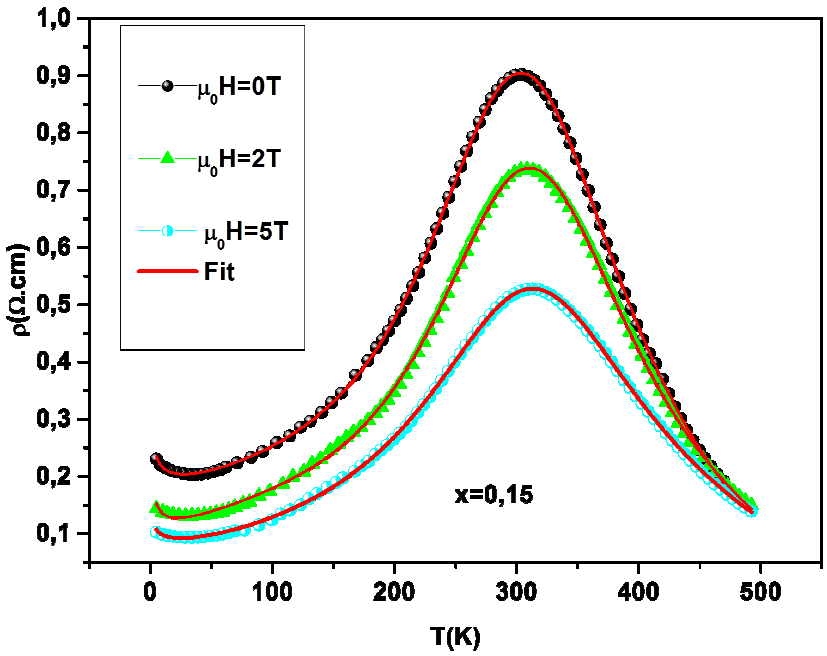

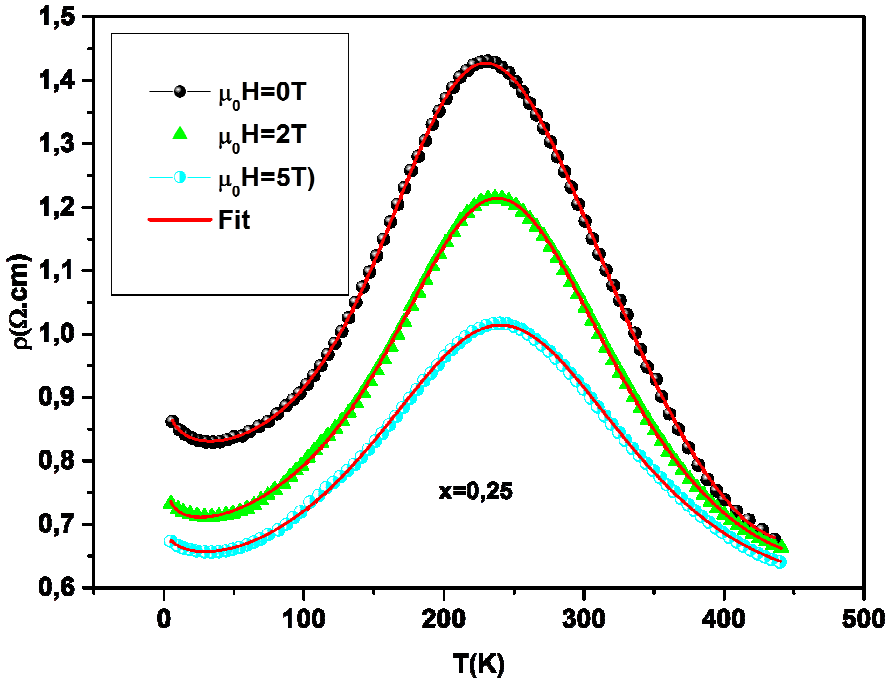

Figure 5

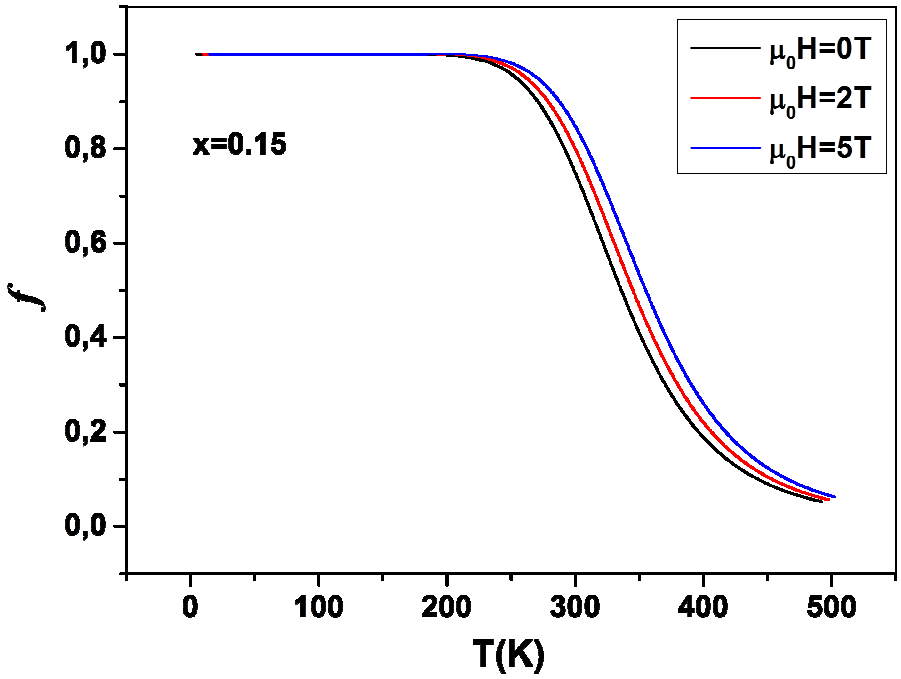

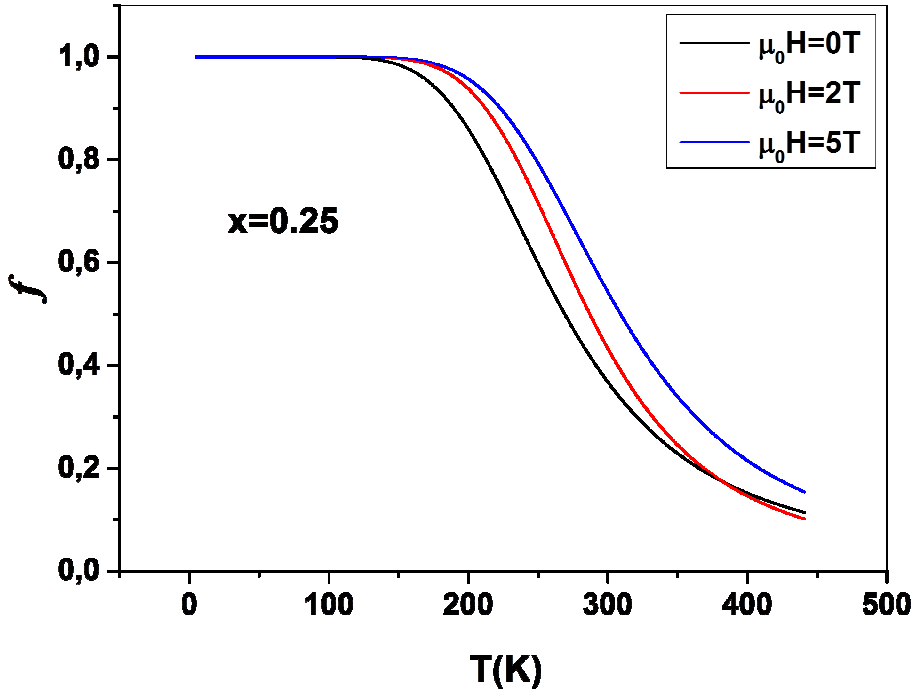

Figure 6

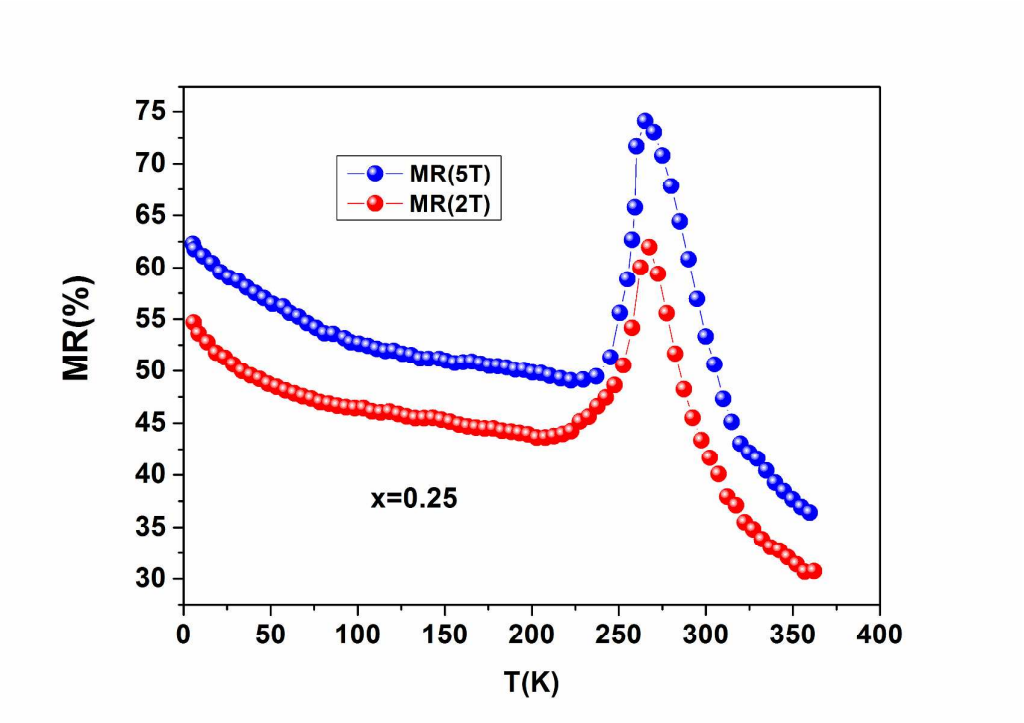

Magnetoresistance plotted vs. temperature for $La_{0.75}Sr_{0.25}Mn_{0.75}Cr_{0.25}O_3$ sample under different magnetic field.